



ALMA MATER STUDIORUM  
UNIVERSITÀ DI BOLOGNA

ARCHIVIO ISTITUZIONALE  
DELLA RICERCA

Alma Mater Studiorum Università di Bologna  
Archivio istituzionale della ricerca

Accurate Damping Factor and Frequency Estimation for Damped Real-Valued Sinusoidal Signals

This is the final peer-reviewed author's accepted manuscript (postprint) of the following publication:

*Published Version:*

Accurate Damping Factor and Frequency Estimation for Damped Real-Valued Sinusoidal Signals / Song, J; Mingotti, A; Zhang, JH; Peretto, L; Wen, H. - In: IEEE TRANSACTIONS ON INSTRUMENTATION AND MEASUREMENT. - ISSN 0018-9456. - ELETTRONICO. - 71:(2022), pp. 6503504.1-6503504.4. [10.1109/TIM.2022.3220300]

*Availability:*

This version is available at: <https://hdl.handle.net/11585/909546> since: 2022-12-13

*Published:*

DOI: <http://doi.org/10.1109/TIM.2022.3220300>

*Terms of use:*

Some rights reserved. The terms and conditions for the reuse of this version of the manuscript are specified in the publishing policy. For all terms of use and more information see the publisher's website.

This item was downloaded from IRIS Università di Bologna (<https://cris.unibo.it/>).  
When citing, please refer to the published version.

(Article begins on next page)

This is the final peer-reviewed accepted manuscript of:

**J. Song, A. Mingotti, J. Zhang, L. Peretto and H. Wen, "Accurate Damping Factor and Frequency Estimation for Damped Real-Valued Sinusoidal Signals," in *IEEE Transactions on Instrumentation and Measurement*, vol. 71, pp. 1-4, 2022, Art no. 6503504.**

The final published version is available online at:

<https://doi.org/10.1109/TIM.2022.3220300>

Terms of use:

Some rights reserved. The terms and conditions for the reuse of this version of the manuscript are specified in the publishing policy. For all terms of use and more information see the publisher's website.

*This item was downloaded from IRIS Università di Bologna (<https://cris.unibo.it/>)*

***When citing, please refer to the published version.***

# Accurate Damping Factor and Frequency Estimation for Damped Real-valued Sinusoidal Signals

Jian Song, *Student Member*, Alessandro Mingotti, *Member, IEEE*, Junhao Zhang, *Member, IEEE*, Lorenzo Peretto, *Senior Member, IEEE*, and He Wen, *Senior Member, IEEE*

**Abstract**—The interpolated discrete Fourier transform (IpDFT) is one of the most popular techniques to estimate the parameters of a damped real-valued sinusoidal signal (DRSS). However, its accuracy is affected by strong noise presence and short observation windows. To this end, this letter proposes a novel two-point IpDFT method, called I2pZDFT, for the parameter estimation of a DRSS. The proposed I2pZDFT uses the zero-padding technique to increase the sampling rate in the frequency domain. The conjugate symmetry and the parity of the zero-padded signal are utilized to eliminate the influence of the spectral leakage. Simulation results highlight that the proposed I2pZDFT outperforms the existing IpDFT-based methods in terms of noise immunity, especially in the case of observation windows as short as  $0.5 \sim 1$  cycles.

**Index Terms**—Damped real-valued sinusoidal signal, discrete Fourier transform, parameter estimation, spectral leakage.

## I. INTRODUCTION

MOST nonstationary behaviors in mechanical and power systems are modeled by the damped real-valued sinusoidal signals (DRSS). Fast and accurate estimation of DRSS's parameters is of great importance for system status assessment, fault diagnosis, and event localization [1-4]. For this purpose, both time- and frequency-domain methods have been proposed in previous studies.

The time-domain methods, such as the Prony method [5], Matrix Pencil [6, 7], and estimation of signal parameters via rotational invariance techniques (ESPRIT) [8, 9], provide accurate estimates only if a proper model order is adopted. One of the most popular frequency-domain methods is based on the interpolated discrete Fourier transform (IpDFT) [10-13]. They are not only highly efficient in computation, but also mitigate the fence effect to a certain extent. However, the effects of spectral leakage remain a key limiting factor for such a method. It is difficult to fully compensate for the spectral leakage due to the negative spectrum not being considered in the derivation process. To this end, three-point and two-point IpDFT methods,

Manuscript received 05 August 2022; revised 11 September 2022 and 13 October 2022; accepted 28 October 2022. This work was supported in part by the National Natural Science Foundation of China under Grant 61771190, in part by the science and technology innovation Program of Hunan Province under Grant 2021RC4020, in part by the China Scholarship Council under Grant 202006130143, and in part by the Postgraduate Scientific Research Innovation Project of Hunan Province under Grant QL20210102. (Corresponding author: He Wen.)

Jian Song, Junhao Zhang, and He Wen are with the College of Electrical and Information Engineering, Hunan Province Key Laboratory of Intelligent Electrical Measurement and Application Technology, Hunan University, Changsha 410082, China (e-mail: songjian1705@126.com; luoyzjh@163.com; he\_wen82@126.com).

Alessandro Mingotti and Lorenzo Peretto are with the Department of Electric, Electronic and Information Engineering "G.Marconi," University of Bologna, 40136 Bologna, Italy (e-mail: alessandro.mingotti2@unibo.it; lorenzo.peretto@unibo.it).

named I3pNDFT and I2pNDFT, have been recently proposed in [14] and [15], respectively. Both the I3pNDFT and the I2pNDFT completely eliminate the effects of spectral leakage by using the negative frequency part, and can be regarded as unbiased estimators. However, the accuracy of the I3pNDFT and the I2pNDFT (i) have advantages and disadvantages compared to each other when the adopted window length is a multiple of 0.5 cycles; and (ii) are heavily affected by noise, especially when observation window length is less than 1 cycle.

In this letter a novel two-point IpDFT method, named as I2pZDFT, is proposed to estimate the damping factor and frequency of DRSS. The zero-padding technique is first used in the I2pZDFT, primarily to obtain a finer spectral characteristic in the case of short observation windows and result in higher anti-noise behavior. The conjugate symmetry and parity of the zero-padded signal are used to eliminate the influence of both short and long-range spectral leakage caused by positive and negative frequencies. Finally, the accuracy of the I2pZDFT is analyzed and the advantages of the I2pZDFT with respect to the state-of-the-art estimators are highlighted.

## II. THE PROPOSED I2pZDFT METHOD

Let us consider the sampled DRSS of length  $N$  as:

$$\begin{aligned} x(n) &= s(n) + \varepsilon(n) \\ &= Ae^{\beta n} \cos\left(\frac{2\pi}{N} \lambda_0 n + \phi\right) + \varepsilon(n), \quad n \in [0, N-1] \end{aligned} \quad (1)$$

where  $\beta$ ,  $\lambda_0$ ,  $A$ , and  $\phi$  are the damping factor, the normalized frequency, the amplitude, and the initial phase, respectively, of the DRSS;  $\varepsilon(n)$  represents the white Gaussian noise. Note that the normalized frequency  $\lambda_0$  corresponding to the frequency  $f_0 = \lambda_0 f_s / N$  of the DRSS and angular frequency  $\omega_0 = 2\pi\lambda_0 / N$ , where  $f_s$  denotes sampling rate.

To reduce the sampling intervals in the frequency domain,  $N$  zero samples are padded after the  $N$  samples of the DRSS. Then the  $2N$ -point DFT bins for the  $N$ -point samples of the DRSS, adopting a rectangular window and ignoring the interference from the noise, can be calculated as:

$$V(k) = \frac{A}{2} \left( \frac{e^{j\phi} (1 - (-1)^k \hbar^N)}{1 - \hbar e^{-j\omega_k}} + e^{-j\phi} \frac{1 - (-1)^k \hbar^{*N}}{1 - \hbar^* e^{-j\omega_k}} \right), \quad (2)$$

where  $k = 0, 1, \dots, N_z - 1$ ,  $N_z = 2N$ ,  $\omega_k = 2\pi k / N_z$ ,  $\hbar = e^{\beta + j\omega_0}$ . and  $(\cdot)^*$  is the conjugate operation. On account of  $\hbar \cdot \hbar^* = e^{2\beta}$  and  $\hbar + \hbar^* = 2e^\beta \cos(\omega_0)$ , the equation (2) can be rewritten as:

$$V(k) = \frac{(P_k + P_k^*) - (\hbar^* P_k + \hbar P_k^*) e^{-j\omega_k}}{(1 - 2e^\beta \cos(\omega_0)) e^{-j\omega_k} + e^{2\beta} e^{-j2\omega_k}}, \quad (3)$$

where  $P_k = \frac{A}{2} e^{j\phi} (1 - (-1)^k \hbar^N)$ .

Assuming integer  $k_2 = k_1 + 2$  (Note that  $k_1$  and  $k_2$  are variables, they do not correspond to the second and third bins in (2)), the following equations can then be obtained according to (3):

$$\begin{cases} (P_{k_1} + P_{k_1}^*) - (\hat{h}^* P_{k_1} + \hat{h} P_{k_1}^*) e^{-j\omega_{k_1}} \\ = V(k_1) (1 - 2e^\beta \cos(\omega_0) e^{-j\omega_{k_1}} + e^{2\beta} e^{-j2\omega_{k_1}}) \\ (P_{k_2} + P_{k_2}^*) - (\hat{h}^* P_{k_2} + \hat{h} P_{k_2}^*) e^{-j\omega_{k_2}} \\ = V(k_2) (1 - 2e^\beta \cos(\omega_0) e^{-j\omega_{k_2}} + e^{2\beta} e^{-j2\omega_{k_2}}) \end{cases} \quad (4)$$

It is clear that  $P_{k_1} = P_{k_2}$  because  $k_1$  and  $k_2$  have the same odd or even nature. Let  $P = P_{k_1} = P_{k_2}$ ,  $\Phi = 1/(e^{-j\omega_{k_1}} - e^{-j\omega_{k_2}})$ ,  $a = e^\beta \cos(\omega_0)$  and  $b = e^\beta \sin(\omega_0)$ . After some manipulation on (4),  $P$  and  $P^*$  can be rewritten as:

$$\begin{cases} P = \frac{\Phi}{j2b} (g(1 - (a + jb)e^{-j\omega_{k_2}}) - h(1 - (a + jb)e^{-j\omega_{k_1}})) \\ P^* = \frac{\Phi}{j2b} (h(1 - (a - jb)e^{-j\omega_{k_1}}) - g(1 - (a - jb)e^{-j\omega_{k_2}})) \end{cases} \quad (5)$$

where:

$$\begin{cases} g = V(k_1) (1 - 2ae^{-j\omega_{k_1}} + e^{2\beta} e^{-j2\omega_{k_1}}) \\ h = V(k_2) (1 - 2ae^{-j\omega_{k_2}} + e^{2\beta} e^{-j2\omega_{k_2}}) \end{cases} \quad (6)$$

Adding or subtracting  $P^*$  from  $P$ , respectively, yields the following equations:

$$P + P^* = \Phi (he^{-j\omega_{k_1}} - ge^{-j\omega_{k_2}}), \quad (7)$$

$$P - P^* = \frac{\Phi}{jb} ((g - h) + a(he^{-j\omega_{k_1}} - ge^{-j\omega_{k_2}})), \quad (8)$$

and equation (8) can be rewritten as:

$$jb(P - P^*) = \Phi(g - h) + a(P + P^*). \quad (9)$$

Because  $P$  and  $P^*$  are conjugately equal, one obtains:

$$\text{Im}[P + P^*] = 0, \quad \text{Re}[P - P^*] = 0, \quad (10)$$

where  $\text{Re}[\ ]$  and  $\text{Im}[\ ]$  return the real and imaginary parts of their argument, respectively. Considering that both  $a$  and  $b$  are real values, the equations (7) – (10) can be combined to obtain:

$$\text{Im}[\Phi(g - h)] = 0, \quad \text{Im}[\Phi(he^{-j\omega_{k_1}} - ge^{-j\omega_{k_2}})] = 0. \quad (11)$$

Substituting (6) into (11), two equations can be simplified as:

$$\begin{cases} aq_{13} = q_{11} + e^{2\beta} q_{12} \\ aq_{23} = q_{21} + e^{2\beta} q_{22} \end{cases}, \quad (12)$$

where:

$$\begin{cases} q_{11} = \text{Im}[\Phi(V(k_2)e^{-j\omega_{k_1}} - V(k_1)e^{-j\omega_{k_2}})] \\ q_{12} = \text{Im}[\Phi(V(k_2)e^{-j\omega_{k_1}}e^{-j2\omega_{k_2}} - V(k_1)e^{-j\omega_{k_2}}e^{-j2\omega_{k_1}})] \\ q_{13} = \text{Im}[2\Phi(V(k_2) - V(k_1))e^{-j\omega_{k_2}}e^{-j\omega_{k_1}}] \\ q_{21} = \text{Im}[\Phi(V(k_1) - V(k_2))] \\ q_{22} = \text{Im}[\Phi(V(k_1)e^{-j2\omega_{k_1}} - V(k_2)e^{-j2\omega_{k_2}})] \\ q_{23} = \text{Im}[2\Phi(V(k_1)e^{-j\omega_{k_1}} - V(k_2)e^{-j\omega_{k_2}})] \end{cases} \quad (13)$$

By solving the linear equations (12) in two unknowns, the estimated  $a$  and damping factor  $\beta$  can be calculated as following:

$$\hat{a} = ((q_{11}q_{22} - q_{12}q_{21}) / (q_{13}q_{22} - q_{12}q_{23})), \quad (14)$$

$$\hat{\beta} = \frac{1}{2} \ln((q_{11}q_{23} - q_{13}q_{21}) / (q_{13}q_{22} - q_{12}q_{23})), \quad (15)$$

and the normalized frequency  $\lambda_0$  can then be estimated as:

$$\hat{\lambda}_0 = \arccos(\hat{a}/e^{\hat{\beta}}). \quad (16)$$

Generally, any two bins whose indexes have the same odd or even nature can be used under noise-free conditions. For maximum noise immunity, the two bins with the highest magnitude among all alternatives are recommended. Considering the denominator  $(q_{13}q_{22} - q_{12}q_{23})$  in (14) and (15) is equal to 0 when  $k_1 = 0$  since the imaginary part of the first bin is zero. Let  $k_m$  be the index of the highest DFT bin. The optimal selection of the two bins is as follows:

$$\begin{cases} k_1 = 1, & k_2 = 3, & \text{when } k_m = 0, 1 \\ k_1 = k_m - 1, & k_2 = k_m + 1, & \text{when } k_m \geq 2 \end{cases} \quad (17)$$

Finally, the implementation steps of the proposed I2pZDFT are concluded as follows:

Step 1: obtain sequence  $x(n)$  with  $N$  samples of DRSS signal;  
Step 2: generate  $2N$ -point sequence  $x_z(n)$  by padding  $N$  zero samples after the  $x(n)$ ;

Step 3: obtain  $2N$ -point DFT bins, i.e.,  $V(k)$  in (2), by executing the fast Fourier transform (FFT) on the  $x_z(n)$ ;

Step 4: calculate the magnitude of  $V(k)$ , then let  $k_m$  be the index of the highest DFT bin;

Step 5: determine the values of  $k_1$  and  $k_2$  based on (17);

Step 6: calculate process parameters (i.e.,  $q_{11}$ ,  $q_{12}$ ,  $q_{13}$ ,  $q_{21}$ ,  $q_{22}$ , and  $q_{23}$ ) based on (13);

Step 7: calculate damping factor  $\hat{\beta}$  and normalized frequency  $\hat{\lambda}_0$  based on (14), (15) and (16); and the frequency can be obtain by  $\hat{f}_0 = \hat{\lambda}_0 f_s / N$ .

### III. BEHAVIOR OF THE I2pZDFT METHOD

#### A. Accuracy Analysis by Simulation

Simulations are conducted to evaluate the effectiveness and robustness of the proposed I2pZDFT method. To demonstrate the behavior of the proposed I2pZDFT method, it has been compared with I3pNDFT [14] and I2pNDFT [15]. This is because it has been proven that they outperform other DFT-based methods in [14] and [15]. For each run, the test signal's amplitude  $A$  is 1, and the initial phase  $\phi$  is a random value in the range of  $[0, 2\pi)$  rad. All simulation results are obtained from the statistics of 10,000 independent runs. The behaviors of the methods are compared according to the mean square error (MSE), which can be calculated from:

$$\text{MSE}(\kappa) = 10 \log_{10} \left\{ \frac{1}{M} \sum_{i=1}^M (\hat{\kappa}(i) - \kappa)^2 \right\}, \quad (18)$$

where  $\kappa$  denotes the actual value of the damping factor  $\beta$  or the normalized frequency  $\lambda_0$ .  $\hat{\kappa}(i)$  is the estimated value of the  $i$ th independent trial corresponding to the actual value. The MSE's quantity is represented in dB when compared with respect to the latest IpDFT methods.

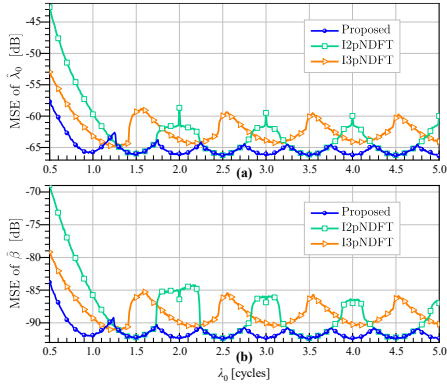


Fig. 1. MSE vs  $\lambda_0$  when  $SNR=40\text{dB}$ ,  $\beta=10^{-4}$ , and  $N=128$ : (a)  $\hat{\lambda}_0$ ; (b)  $\hat{\beta}$ .

Fig. 1 reports MSEs of the results returned by methods when the normalized frequency  $\lambda_0$  (corresponding to the window length) changes from 0.5 to 5 cycles with a 0.01 cycles step. Other parameters are set as  $N = 128$ ,  $SNR = 40$  dB, and  $\beta = 10^{-4}$ . The results show that the I2pZDFT provides the smallest MSEs among the three methods in most cases. When the length of adopted window  $\nu > 1.3$  cycles, the I2pZDFT consistently outperforms the I3pNDFT. The MSEs of the I2pZDFT are 5 dB smaller than those of the I2pNDFT when  $\nu$  is near an integer.

Fig. 2 reports MSEs of the results obtained when the damping factor  $\beta$  varies from  $-0.04$  to  $0.04$  with a 0.001 step. Other parameters are set as  $N = 128$ ,  $SNR = 40$  dB, and  $\lambda_0 = 0.9$  cycles. As shown in Fig. 2, the MSE values increase with the absolute value of  $\beta$ , and the I2pZDFT provides the smallest MSEs among the three methods. When  $|\beta| = 0.04$ , the MSEs corresponding to  $\hat{\lambda}_0$  and  $\hat{\beta}$  of the I2pZDFT are smaller than those of the I2pNDFT of 1.5 and 3 dB, respectively.

Fig. 3 reports MSEs of the results returned by methods when the noise level  $SNR$  varies from 0 to 70 dB with a 1 dB step. Other parameters are set as  $N = 128$ ,  $\lambda_0 = 0.9$  cycles, and  $\beta = 10^{-4}$ . It can be observed that the I2pZDFT outperforms both the other two methods. The MSEs of  $\hat{\lambda}_0$  and  $\hat{\beta}$  of the I2pZDFT are smaller than those of the I2pNDFT of 8 and 8.6 dB, respectively. The MSEs of  $\hat{\lambda}_0$  and  $\hat{\beta}$  of the I2pZDFT are smaller than those of the I3pNDFT of 3.8 and 4 dB, respectively.

Fig. 4 reports MSEs of the results returned by methods when the initial phase  $\phi$  varies from  $-\pi$  to  $\pi$  rad with a  $\pi/180$  step. Other parameters are set as  $N = 128$ ,  $SNR = 40$  dB,  $\lambda_0 = 0.9$  cycles, and  $\beta = 10^{-4}$ . As reported in Fig. 4, the I2pZDFT is

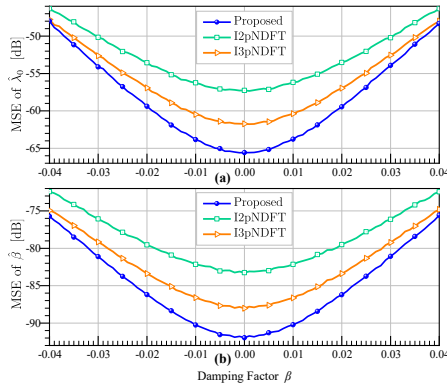


Fig. 2. MSE vs  $\beta$  when  $SNR=40\text{dB}$ ,  $\lambda_0=0.9$ , and  $N=128$ : (a)  $\hat{\lambda}_0$ ; (b)  $\hat{\beta}$ .

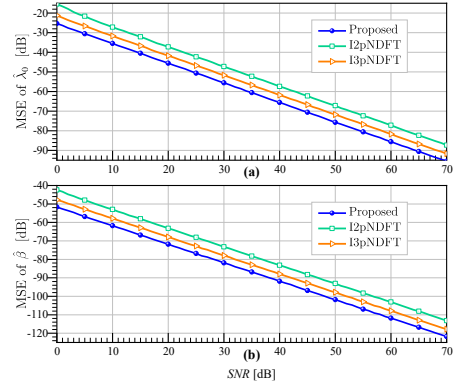


Fig. 3. MSE vs  $SNR$  when  $\beta=10^{-4}$ ,  $\lambda_0=0.9$ , and  $N=128$ : (a)  $\hat{\lambda}_0$ ; (b)  $\hat{\beta}$ .

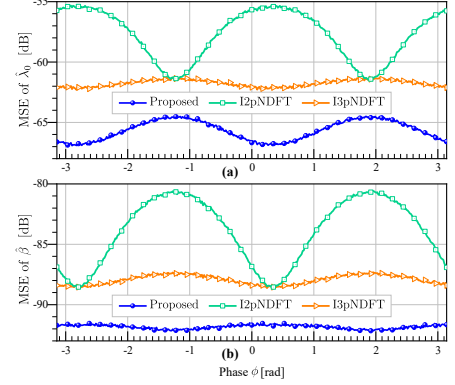


Fig. 4. MSE vs  $\phi$  when  $SNR=40\text{dB}$ ,  $\beta=10^{-4}$ ,  $\lambda_0=0.9$ , and  $N=128$ : (a)  $\hat{\lambda}_0$ ; (b)  $\hat{\beta}$ . slightly influenced by the phase fluctuation and outperforms both the I2pNDFT and the I3pNDFT. However, the behavior of the I2pNDFT is dramatically influenced by the phase fluctuation. The MSEs of  $\hat{\lambda}_0$  and  $\hat{\beta}$  of the I2pZDFT are at least 3 dB smaller than those of the other two methods.

In fact, longer windows do not always mean better anti-noise behavior as the noise may obscure the contribution of the damping factor with an increase in the observation window. Fig. 5 reports MSEs of the results returned by the I2pZDFT when the number of the samples  $N$  varies from 32 to 256. Other parameters are set as  $SNR = 40$  dB and  $\lambda_0 = 0.9$  cycles in which three different damping factors are considered. The accuracy of the I2pZDFT decreased as the window length increases when  $\beta = 0.02$ . However, this phenomenon does not appear when  $\beta = 0.01$  or  $\beta = 10^{-4}$ . Hence, the effect  $\beta$  should be considered when choosing the window length in the actual measurement.

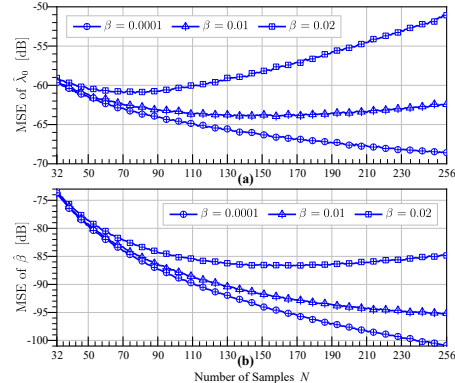


Fig. 5. MSE vs  $N$  and  $\beta$  when  $SNR=40\text{dB}$  and  $\lambda_0=0.9$ : (a)  $\hat{\lambda}_0$ ; (b)  $\hat{\beta}$ .

### B. Parameters Estimation of Oscillation in Power Systems

The behavior of the I2pZDFT is also verified using ringdown signal (i.e., a kind of oscillation signals) in the power system, whose data can be obtained in [16]. Here, the last 10 second signal with a sampling rate of 30 Hz at bus angle 11 is leveraged for analysis. In such a scenario, a three-phase short circuit fault caused a dominant mode with 0.7036 Hz frequency and -0.0017 normalized damping factor. The estimated results provided by the I2pZDFT are listed in Table I. The absolute errors of frequency estimation offered by the I2pZDFT, the I2pNDFT, and the I3pNDFT are 0.3, 1.8, and 0.9 mHz, respectively. As for the damping factor, both the I2pZDFT and the I3pNDFT has the same estimation error but more accurate than the I2pNDFT. Overall, the I2pZDFT outperforms the other two methods in estimation of the dominant mode of oscillation signal.

TABLE I PARAMETERS OF DOMINANT MODE

Parameters	I2pZDFT	I2pNDFT	I3pNDFT	Ref Value
Frequency [Hz]	0.7039	0.7054	0.7027	0.7036
Damping factor	-0.0015	-0.0021	-0.0015	-0.0017

### C. Computational Complexity

The computational complexity of three methods is analyzed in Table II. The heaviest computational burden comes from FFT part. The I2pZDFT requires more computation than the other two methods because the I2pZDFT needs to calculate  $N_z$  (i.e.,  $2N$ ) point DFT bins. This indicates that the I2pZDFT obtains better noise immunity at the cost of increased computational burden. However, it is still lighter than non-DFT-based estimators, e.g., ESPRIT, and Matrix Pencil.

TABLE II COMPUTATIONAL COMPLEXITY

Method	FFT	+	-	×	÷	sqrt	log	exp	cos <sup>-1</sup>
I2pZDFT	$O(N_z \log_2 N_z)$	6	14	3	1	1	1	1	1
I2pNDFT	$O(N \log_2 N)$	8	12	6	0	1	1	1	1
I3pNDFT	$O(N \log_2 N)$	26	12	3	1	1	1	0	1

The computational burden is also analysed using simulations in MATLAB R2019b running on a laptop with 16-GB RAM and a 2.3-GHz processor. In tests,  $N = 32, 64, 128, 256, 512$  are considered. The total execution time of 100,000 runs is reported in Table III. Although the I2pZDFT is heavier than the other two methods, the average execution time of the I2pZDFT is still a tiny value. This indicates that it is still suitable for application in scenarios where high computational efficiency is required.

TABLE III TOTAL EXECUTION TIME OF 100,000 RUNS IN SECONDS

Method	$N=32$	$N=64$	$N=128$	$N=256$	$N=512$
I2pZDFT	2.924 s	3.198 s	3.566 s	4.993 s	6.489 s
I2pNDFT	1.785 s	1.912 s	2.234 s	3.223 s	4.313 s
I3pNDFT	1.883 s	2.004 s	2.390 s	3.395 s	4.198 s

## IV. CONCLUSION

In this work, a novel two-point IpDFT method was proposed for damping factor and frequency estimation of DRSS. Thanks to (i) the noise immunity is enhanced by using the  $N$  points zero-padding technique; (ii) the conjugate symmetry and the parity of the zero-padded signal are used to eliminate the influence of both short and long-range spectral leakage; (iii) the rectangular window has the smallest equivalent noise bandwidth among all

windows. The proposed I2pZDFT has high accuracy and outperforms the existing IpDFT-based methods. Its MSEs are almost 15 dB smaller than the I2pNDFT when the length of the observation window is 0.5 cycles.

## REFERENCES

- [1] S. Tomar, and P. Sumathi, "Amplitude and Frequency Estimation of Exponentially Decaying Sinusoids," *IEEE Transactions on Instrumentation and Measurement*, vol. 67, no. 1, pp. 229-237, 2018.
- [2] M. Mansouri, M. Mojiri, M. A. Ghadiri-Modarres, and M. Karimi-Ghartemani, "Estimation of Electromechanical Oscillations From Phasor Measurements Using Second-Order Generalized Integrator," *IEEE Transactions on Instrumentation and Measurement*, vol. 64, no. 4, pp. 943-950, Apr, 2015.
- [3] R. C. Wu, and C. T. Chiang, "Analysis of the Exponential Signal by the Interpolated DFT Algorithm," *IEEE Transactions on Instrumentation and Measurement*, vol. 59, no. 12, pp. 3306-3317, Dec, 2010.
- [4] Y. L. Zhu, C. X. Liu, and L. Z. Yao, "A Faster Estimation Method for Electromechanical Oscillation Frequencies," *IEEE Transactions on Power Systems*, vol. 34, no. 4, pp. 3280-3282, Jul, 2019.
- [5] G. W. Chang, and C.-I. Chen, "An Accurate Time-Domain Procedure for Harmonics and Interharmonics Detection," *IEEE Transactions on Power Delivery*, vol. 25, no. 3, pp. 1787-1795, 2010.
- [6] L. Bernard, S. Goondram, B. Bahrani, A. Pantelous, and R. Razzaghi, "Harmonic and Interharmonic Phasor Estimation using Matrix Pencil Method for Phasor Measurement Units," *IEEE Sensors Journal*, pp. 1-1, 2020.
- [7] J. Song, J. Zhang, and H. Wen, "Accurate Dynamic Phasor Estimation by Matrix Pencil and Taylor Weighted Least Squares Method," *IEEE Transactions on Instrumentation and Measurement*, vol. 70, pp. 1-11, 2021.
- [8] S. K. Jain, and S. N. Singh, "Exact Model Order ESPRIT Technique for Harmonics and Interharmonics Estimation," *IEEE Transactions on Instrumentation and Measurement*, vol. 61, no. 7, pp. 1915-1923, 2012.
- [9] S. K. Jain, P. Jain, and S. N. Singh, "A Fast Harmonic Phasor Measurement Method for Smart Grid Applications," *IEEE Transactions on Smart Grid*, vol. 8, no. 1, pp. 493-502, 2017.
- [10] K. Duda, L. B. Magalas, M. Majewski, and T. P. Zielinski, "DFT-based Estimation of Damped Oscillation Parameters in Low-Frequency Mechanical Spectroscopy," *IEEE Transactions on Instrumentation and Measurement*, vol. 60, no. 11, pp. 3608-3618, Nov, 2011.
- [11] R. Diao, and Q. Meng, "An Interpolation Algorithm for Discrete Fourier Transforms of Weighted Damped Sinusoidal Signals," *IEEE Transactions on Instrumentation and Measurement*, vol. 63, no. 6, pp. 1505-1513, 2014.
- [12] X. M. Yang, J. N. Zhang, X. R. Xie, X. Y. Xiao, B. Gao, and Y. Wang, "Interpolated DFT-Based Identification of Sub-Synchronous Oscillation Parameters Using Synchronphasor Data," *IEEE Transactions on Smart Grid*, vol. 11, no. 3, pp. 2662-2675, May, 2020.
- [13] K. Duda, and S. Barczentewicz, "Interpolated DFT for sin(alpha)(x) Windows," *IEEE Transactions on Instrumentation and Measurement*, vol. 63, no. 4, pp. 754-760, Apr, 2014.
- [14] K. Wang, H. Wen, W. S. Tai, and G. Q. Li, "Estimation of Damping Factor and Signal Frequency for Damped Sinusoidal Signal by Three Points Interpolated DFT," *IEEE Signal Processing Letters*, vol. 26, no. 12, pp. 1927-1930, Dec, 2019.
- [15] K. Wang, H. Wen, L. Xu, and L. Wang, "Two Points Interpolated DFT Algorithm for Accurate Estimation of Damping Factor and Frequency," *IEEE Signal Processing Letters*, vol. 28, pp. 499-502, 2021.
- [16] S. Maslennikov, B. Wang, Q. Zhang, F. Ma, X. C. Luo, K. Sun, and E. Litvinov, "A Test Cases Library for Methods Locating the Sources of Sustained Oscillations," *2016 IEEE Power and Energy Society General Meeting (PESGM)*, 2016.